JOURNAL OF THERMOPHYSICS AND HEAT TRANSFER
Vol. 16, No. 1, January–March 2002

# Modeling of Ultraviolet Radiation in Steady and Transient High-Altitude Plume Flows

S. F. Gimelshein*
*George Washington University, Washington, D.C. 20052*
D. A. Levin†
*Pennsylvania State University, University Park, Pennsylvania 16802*
J. A. Drakes‡
*Arnold Engineering Development Center, Arnold Air Force Base, Tennessee 37389-9900*
and
G. F. Karabadzhak§ and Yu. Plastinin¶
*TsNIIMASH, 141070, Korolev, Russia*

**Ultraviolet radiation from hydrazine spacecraft thruster plumes interacting with ambient atomic oxygen is modeled for low-Earth-orbit conditions. Two numerical techniques that employ the direct simulation Monte Carlo method are applied for the first time to the modeling of space plume radiation transient and three-dimensional flows. These efficient procedures allow one to analyze the effect of atomic oxygen penetration of the thruster plume, which is a key factor in modeling rarefied space plume radiation. The overlay technique is used to model the transient flow evolution during the first several seconds after motor ignition. Good agreement between modeling and experiment are obtained before 1-s motor burn time. The sensitivity of the plume radiation to the molecular total collision model is analyzed using the overlay technique, and the radiation spatial distribution was found to be strongly dependent on the temperature exponent of the coefficient of viscosity. Three-dimensional computations are conducted for different angles between the plume axis and the freestream directions, and the radiation maps for OH($A$) and NH($A$) are presented. Significant difference between OH($A$) and NH($A$) radiation fields as a function of the angle of attack is shown.**

## I. Introduction

THE modeling of radiation from high-altitude spacecraft thruster plumes in low Earth orbit is a challenging task requiring efficient and new algorithms to study fundamental plume physics and to enable comparisons with experimental imagery and spectral radiation data. Ultraviolet radiation is formed in high-altitude thruster plumes through chemiluminescent reactions between thrust plume species such as water or hydrazine fragments and ambient atomic oxygen species with orbital velocities. Therefore, the accurate modeling of atomic oxygen penetration of the thruster plume is a key factor in modeling rarefied space plume radiation. The penetration will be related to the elastic scattering total cross section and three-dimensional, angle of attack geometry. When a collision occurs between the plume species and atomic oxygen, the probability of a reaction will depend on the Arrhenius parameters, especially the reaction threshold. Some of the molecular collision parameters can be obtained from the fundamental chemical physics literature. However, the collision conditions that exist in low Earth orbit are sufficiently different such that not all basic elastic and chemical reaction cross section information is available. If accurate and efficient numerical techniques are available, the space environment can be thought of as a laboratory to study fundamental processes involving high-energy chemical collision processes in rarefied flows. A particle approach, such as the direct simulation Monte Carlo (DSMC) method, must be used to model the rarefied nature of the flow.

Two complimentary data sets of UV radiation from hydrazine space plumes in low Earth orbit exist from the shuttle Arizona Airglow Instrument (GLO)[1] and MirEx[2] experiments. These data sets combined provide information about the plume spectral radiation, transient time evolution, and three-dimensional, angle-of-attack characteristics. However, the particle modeling of these plume features is computationally intensive because it requires large numbers of variations of the basic collision parameters, large number of simulated particles for transient flows, and high grid resolution combined with large particle numbers for three-dimensional modeling.

In this work, two different numerical techniques are used to address these questions: 1) an overlay method, a new technique developed to examine transient radiation phenomena, and 2) the use of a starting surface obtained by axisymmetric DSMC code for subsequent three-dimensional DSMC simulations. The goals of the paper are to apply these two computational techniques for the first time to the modeling of radiation phenomena produced by the interaction of high-energy rocket plumes with the rarefied atmosphere and to compare the computational results with available space experimental data. The two space experiments are briefly described subsequently.

The emphasis of the MirEx program has been to obtain calibrated radiance imagery of high-altitude plumes from the UV to the visible spectral region, on liquid propellant systems. The general concept of the experiment was to view the plumes of service spacecraft as they approach and leave the Mir station. The experimental arrangement, instrumentation, and the data have been discussed in detail in earlier work.[2] UV data of the Soyuz main engine burn from the 25 August

Received 15 May 2001; revision received 1 August 2001; accepted for publication 21 August 2001. 

*Senior Research Scientist, Department of Chemistry; gimel@gwu.edu. Member AIAA.
†Associate Professor, Department of Aerospace Engineering; dalevin@psu.edu. Senior Member AIAA.
‡Research Scientist, Sverdrup Technology, Inc. Senior Member AIAA.
§Head of Laboratory, Department of Radiative Processes in Gases. Senior Member AIAA.
¶Head of Department, Department of Radiative Processes in Gases. Member AIAA.

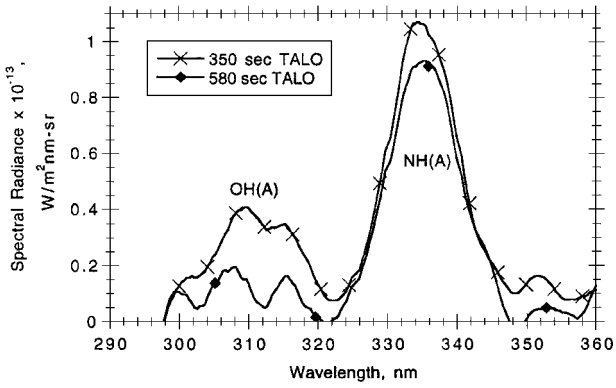


**Fig. 1 Experimental measurements of UV spectrum in the retrofiring configuration of Soyuz main engine.**

1998 and the 28 February 1999 missions were obtained at an altitude of about 380 km, a slant range from the Soyuz to the Mir of 20 km, and a viewing angle with respect to the plume axis of about 10 deg during the retrofiring.[2] The data were acquired by a UV imager with multiple filters, one of which had a bandpass from 265 to 320 nm. An example of spectra obtained during a subsequent mission (26 April 2000) for two different firing times is shown in Fig. 1. The spectra clearly show the presence of both the OH($A$) and NH($A$) radiators in the plume. Note, however, that spectral bandpass of the UV imager emphasizes the radiation from the OH($A$) species. As we discussed in earlier work,[2] the first source comes from the high-energy atomic oxygen collisional dissociation of water, a main plume species. The source of NH($A$) radiation comes from the excitation of hydrazine fragments by collisions with atomic oxygen.

UV data also exist from the shuttle flight experiments of the shuttle primary reaction control system (PRCS) engines in a flight regime very similar to that of MirEx. The altitudes of the firings of the shuttle PRCS engines and the Progress Main Engine (PME) are 290–360 km vs approximately 370 km, both firing into essentially the same space environment.[1] The propellants and thrust levels of both engines are similar. The PRCS uses a monomethyl hydrazine instead of the unsymmetrical d-methylhydrazine (UDMH) propellant of the PME with the difference that the latter is doubly substituted with a methyl radical. Onboard spectroscopic data were taken with the GLO instrument on flights STS 53 in December 1992 and STS 63 in February 1995.[1] Spectral data were presented for a distance of 4, 10, and 33 m from the thruster nozzle. Hence, in contrast to the MirEx data, the measurements emphasize only the plume region close to the nozzle. The spectra at 4 m show the presence of NH($A \rightarrow X$) radiation, whereas a scan at 33 m shows additional radiation from OH($A \rightarrow X$).

In previous work[2] we sought to develop an efficient, accurate simulation technique suitable for modeling chemiluminescent reactions in rarefied flows with axial symmetry. The modeling is challenging due to the variable flow length scales and resolution of infrequent reactions events that lead to radiation. Because the flow regime is rarefied, the simulation technique used is the DSMC method.[3] We have shown that careful attention must be paid to numerical issues such as grid resolution and particle number convergence.

However, the past work left several remaining issues. The reason for the factor of 20 overprediction of the modeling compared to the MirEx data could not be resolved. It also did not seek to understand the potential phenomenology and modeling improvements that might be available by comparison with the MirEx plume transient data. The shuttle GLO data provide data about variation of UV radiation with angle of attack. To model such data requires highly accurate three-dimensional simulations that are not possible unless a starting surface technique is used. Thus, the past work showed the need for better computational techniques to perform in-depth data analyses and to better understand the fundamental controlling UV radiation. The outline of this paper is as follows. The next section reviews the low-Earth-ambient space environment, the chemical reactions modeled, and the viewing geometry. Section III provides a detailed description of the overlay and starting surface approaches.

**Table 1 Summary of freestream conditions**

| Parameter | Value |
|---|---|
| Temperature | 883 K |
| Number density | $1.34 \times 10^{14}$ molecule/m$^3$ |
| Soyuz-TM velocity | 7350 m/s |
| O mole fraction | 0.909 |
| He mole fraction | 0.0517 |
| $N_2$ mole fraction | 0.0393 |

**Table 2 Rate constant and thermodynamic data**

| Equation $A$, m$^3$ molecule$^{-1}$ s$^{-1}$ | $B$ | $E_a$, eV |
|---|---|---|
| (1) $3.8 \times 10^{-21}$ | 1.3 | 4.8 |
| (2) $2.0 \times 10^{-15}$ | 0 | 2.5 |

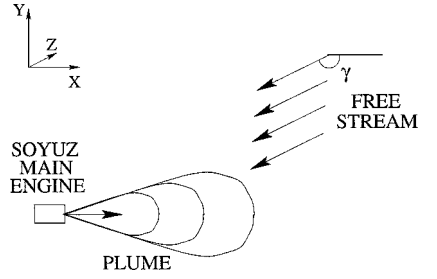


**Fig. 2 Schematic of the flow; angle of attack $\gamma$ = 180 deg represents retrofiring configuration.**

In Sec. IV, results are shown of the overlay technique applied to the modeling of transient plumes and to the modeling of the elastic scattering total cross section in a steady flow. Comparison of the modeled transient radiation with the experimental data is presented. Finally, the three-dimensional angular dependence of the plume radiation is modeled and contrasted for the two different UV radiators and is qualitatively compared with the Shuttle GLO results.

## II. Initial and Boundary Conditions

The typical altitude of the spacecraft during the observations ranged from 360 to 390 km. The freestream conditions used in this study correspond to an altitude of 380 km and are given in Table 1. The plume chemiluminescent chemical reactions considered are

$$H_2O + O \rightarrow OH(A) + OH(X) \quad (1)$$

$$CH_2NH + O \rightarrow NH(A) + H_2CO \quad (2)$$

The rate constants for Eq. (1) have not been measured for the conditions of rarefied space plumes. The rate coefficient for Eq. (2) have been inferred from analyses of shuttle GLO data (private communication with L. S. Bernstein). Table 2 gives the rate constant coefficients defined in terms of the usual Arrhenius parameters as[4]

$$k = AT^B \exp(E_a/kT)$$

The calculations presented in this work are those simulating the Mir experimental imagery data obtained on 25 August 1998. In this mission, the Soyuz-TM vehicle dedocked from Mir and drifted to a position 15 km behind Mir and 2 km above it. The Soyuz-TM motor was ignited at that position. During the retrofiring that lasted over 240 s, the Soyuz-TM decreased altitude from 385 to 375 km, and the angle of attack $\gamma$ increased from 7 to 14 deg (see Fig. 2). To compare modeling with data, the number of reactions per cubic meter per second was integrated through the appropriate lines of sight. This generates arrays of reactions per square meter per second, which is proportional to the integrated radiation field.

## III. Computational Approaches

### A. Numerical Challenges for Kinetic and Continuum Methods

Modeling of high-altitude radiation produced as a result of the interaction between a rocket plume and the ambient atmosphere

represents a significant computational challenge. The computational difficulties are mostly related to the following aspects.

There is strong density variation. The density changes by many orders of magnitude from the nozzle exit to the plume far field. The flow regime is continuum in the vicinity of the nozzle exit, and near free molecular in the ambient atmosphere. This means that a continuum approach has to be used to resolve properly the flow in the vicinity of the plume exit, whereas a kinetic, that is, particle, approach must be applied for modeling the radiative interaction of the plume and the atmosphere. The results of the continuum modeling of the plume near field, therefore, need to be transferred to the subsequent particle simulation through a starting surface.

There is a large spatial scale. Modeling of the plume–atmosphere interaction at low Earth orbit, that is, at an altitude of about 300 km, implies calculation of flows with the gas mean free paths of the order of hundreds of meters. This results in computational domains of large sizes that can reach tens of kilometers.

Radiation events are rare. The radiance is produced as a result of the interaction between plume and atmospheric species. The low density of the atmosphere implies there are few collisions between the plume and atmospheric species, and the reactions that may produce radiation are even more rare. This creates significant computational requirements for particle simulation where good statistics are necessary to draw meaningful conclusions.

There is a need to model transient and three-dimensional phenomena. The accurate modeling of transient processes is traditionally a difficult problem for particle simulations, again due to large, impractical computational requirements. The computational requirements are also severe when the flow may not be represented with a two-dimensional or axisymmetric model, and three-dimensional computations are required.

The following techniques have been used to overcome the mentioned problems. The flow at the exit of Soyuz-TM thruster is quite dense and is certainly not affected by the atmosphere. The small vicinity of the nozzle exit (~30 m) was, therefore, modeled using the continuum approach in an axisymmetric statement. A solution of the Navier–Stokes equations was used for that small region. The Navier–Stokes solution (see Ref. 5) obtained at the distance of 20 m downstream of the nozzle was utilized then as the initial condition (starting surface) for the subsequent DSMC computations. The profiles of the macroparameters of plume velocities in the $X$ and $Y$ directions and number density at 20 m, taken as the input for the DSMC method, are shown in Fig. 3. In Fig. 3, the abscissa $X$ is the distance perpendicular to the rocket-plume axis at 20 m from the nozzle. It is assumed that there are no chemical reactions among the plume effluent species, and therefore, the plume species mole fractions are constant (see Table 3).

The DSMC-based computational tool SMILE[6] is used in this work to study the interaction of the rocket plume with rarefied atmosphere. Special attention was paid to the accuracy of the results obtained. Different two-level Cartesian grids for collisions and macroparameters are used, which enables one to apply different adaption strategies. Radial cell-based weights are employed in all axisymmetric calculations to reduce statistical scatter near the plume axis. Based on our previous research,[7] the computational domain was decreased to 10 km in the direction of the plume and 2 km in the perpendicular direction. Such a decrease enables us to decrease significantly computational requirements while preserving the high accuracy of results.

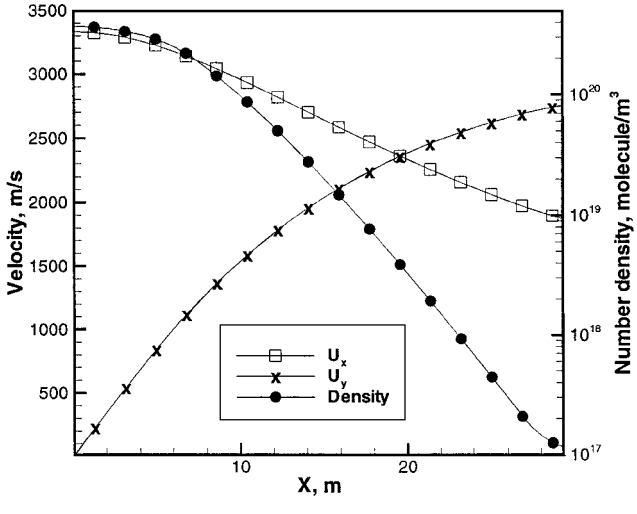


**Fig. 3 Plume macroparameters at 20 m obtained by continuum approach, used as initial conditions for the DSMC calculations.**

**Table 3 Plume species mole fractions[a]**

| Species | Mole fraction |
|---|---|
| $X(H_2O)$ | 0.288 |
| $X(N_2)$ | 0.267 |
| $X(H_2)$ | 0.190 |
| $X(CO)$ | 0.189 |
| $X(CO_2)$ | 0.053 |
| $X(H)$ | 0.013 |
| $X(OH)$ | $1.07 \times 10^{-5}$ |

[a]At 20 m downstream of the nozzle exit.

To avoid problems connected with rare radiation events, a special overlay technique was developed. The details on the technique will be presented in the next section. Here we note only that the statistics issue is especially critical for modeling the transient flow, and the overlay is presumably a good way for obtaining information on transient behavior of radiation map in the rarefied flow.

The following collision models were used in the DSMC computations. The variable hard sphere model[8] was applied for molecular interactions. The Borgnakke–Larsen model[9] with temperature-dependent rotational[10] and vibrational[11] relaxation numbers was assumed for energy transfer between translational and internal molecular modes. The total collision energy model[8] was considered in this work for modeling chemical reactions. For axisymmetric computations, the total number of cells was about 100,000, and the number of molecules was of the order of 400,000. The details on the three-dimensional modeling are given subsequently.

### B. Use of an Overlay Technique

Although the DSMC approach enables one to obtain an accurate solution for flowfields and surface properties, the calculation of radiation is difficult due to a very small number of radiation events even for a large number of simulated molecules. This factor increases the total computational time by orders of magnitude and also prohibits an analysis of the transient plume radiation during the first seconds of motor firing. The main assumptions and features of the overlay technique are given later. The principal idea of the overlay technique is to use the macroparameter fields obtained by the DSMC method, to calculate radiation. Because the statistical scatter is much lower for macroparameters such as density and velocity than for radiative collisions, such an approach, if proved to be applicable, is of great benefit for studying unsteady radiation phenomena. In this work, the overlay technique was applied to model radiation in steady and transient flows in the retrofiring configuration. For this configuration, only $OH(A)$ radiation was considered because it is the dominant radiation source in the MirEx spectral bandpass.[2]

First, let us write the total number of radiation events per second as

$$N_r = n_a n_b \langle \sigma_r(E) g \rangle$$

where $n_a$ and $n_b$ are the number densities of reacting species $a$ and $b$, $E$ is the energy contributed into the reaction, and $\sigma_r$ is the reaction cross section. Note, $E$ in the general case depends on the relative collision velocity $g$ and the internal energy modes. For the radiation process of interest [reaction (1)] species $a$ and $b$ are the plume water molecules and freestream atomic oxygen, respectively.

The general expression for the reaction cross section may be written as

$$\langle \sigma_r(E) g \rangle = \int P(E) \sigma_{\text{tot}}\, g f(E)\, \mathrm{d}E \qquad (3)$$

where $P(E) = \sigma_r/\sigma_{\text{tot}}$ is the reaction probability, $\sigma_{\text{tot}}$ is the total collision cross section, and $f$ is the energy distribution function.

The interaction of the plume with the freestream at high altitudes does not significantly affect the plume core flow because the number density is much larger than that of the freestream. Because the water vibrational and rotational temperatures are less than 100 K, it is reasonable to assume that the relative translational energy gives the dominant contribution to the reaction cross section. In this case, Eq. (3) is reduced to

$$\langle \sigma_r(g)g \rangle = \int_{-\infty}^{\infty}\int_{-\infty}^{\infty} P(g)\sigma_{\text{tot}}\, g f(\boldsymbol{c}_a) f(\boldsymbol{c}_b)\, \mathrm{d}\boldsymbol{c}_a\, \mathrm{d}\boldsymbol{c}_b \qquad (4)$$

where $\boldsymbol{c}_a$ is the Cartesian velocity vector of species $a$ and Eq. (4) represents an integration over six velocity coordinate components.

Finally, we assume that the oxygen atoms have an average speed and temperature throughout the flow corresponding to those in the freestream. With this assumption $\langle \sigma_r(g)g \rangle$ can be written as

$$\langle \sigma_r(g)g \rangle = \int_{-\infty}^{\infty} P(g)\sigma_{\text{tot}}\, g f(\boldsymbol{c}_b)\, \mathrm{d}\boldsymbol{c}_b \qquad (5)$$

where $g$ here and later is the relative collision velocity of a water molecule (an average cell value of water species is used here) and an atomic oxygen that has a freestream velocity and temperature $g = |\boldsymbol{c}_b - \langle \boldsymbol{c}_a \rangle|$.

Substitution of the standard expression for the total collision energy model[8] for $P(g)$ and a variable hard sphere (VHS) expression[8] for $\sigma_{\text{tot}}$ in Eq. (5) gives the final expression

$$N_r = n_a n_b \frac{\epsilon A}{2\pi\Gamma(\frac{3}{2}+B)}\left(\frac{m_r}{2k}\right)^{2-\alpha}\frac{(2-\alpha)^{-\alpha}}{\Gamma(2-\alpha)}\cdot T^{-\frac{3}{2}} \times \int_{-\infty}^{\infty}\left(1-\frac{2E_a}{m_r g^2}\right)^{1-\alpha}\left(\frac{m_r g^2 - E_a}{k}\right)^{B-0.5+\alpha} g^{1-2\alpha} \times \exp\left\{\frac{-m_r g^2}{kT}\right\}\mathrm{d}\boldsymbol{c}_b$$

where $A$, $B$, and $E_a$ are parameters of the Arrhenius equation; $T$ is the free stream temperature; $m_r$ is the reduced mass; $\epsilon$ is 1 for unlike species; and $\alpha$ is the VHS parameter in viscosity–temperature dependence. The preceding integral can easily be evaluated using standard numerical quadrature methods. The integration limits can be set to $(\langle c_{b,i} \rangle - 5c'_b, \langle c_{b,i} \rangle + 5c'_b)$, where $\langle c_{b,i} \rangle$ is the average velocity for the $i$ component of $\boldsymbol{c}_b$ and $c'_b$ is the corresponding thermal velocity. The evaluation of the integral is performed during the post-processing stage and is applied to all macroparameter cells where $n_a$, $n_b$, and $\langle \boldsymbol{c}_a \rangle$ are calculated.

The approach described here may be generalized to the case when the internal energy contribution to the reaction cross section cannot be neglected.

### C. Starting Surface for Three-Dimensional Simulations

The overlay approach was successfully applied to model transient and steady-state radiation phenomena for the retrofiring, that is, axisymmetric, configuration. The overlay analysis becomes more complicated and difficult to implement when the angle between the plume axis and the flow velocity is nonzero. The geometry is three dimensional in this case, and the three-dimensional SMILE computational tool[6] was used in this work to compute radiation maps for steady flows at different angles of attack.

A DSMC computation of three-dimensional flows, especially those with many species, chemical reactions, and large density variations through the flow, is extremely complicated from the numerical point of view. In the previous paper,[7] an attempt to model in detail a three-dimensional plume from the Soyuz main engine interacting with an ambient gas was undertaken for different angles of attack varying from 0 to 180 deg. For the purpose of validation, a comparison was carried out between three-dimensional results for 180 deg and those obtained by the axisymmetric DSMC code. A difference was observed in the density and temperature fields, which was attributed to the influence of grid resolution and the number of simulated particles.

In this work, more detailed calculations were performed with the number of molecules and collision cells of 2 and $10 \times 10^6$, respectively. This is greater than a factor of five improvement compared to Ref. 7. Note that such an improvement enabled us to reduce drastically the difference in flowfields discussed in Ref. 7 for the axisymmetric and three-dimensional DSMC codes. The computations were performed using a parallel capability of the SMILE code. To obtain accurate grid-resolved three-dimensional results, an intermediate axisymmetric DSMC computation of the plume flow from 20 to 1000 m downstream of the nozzle exit was obtained. The results of the axisymmetric computation were used to produce a starting surface for three-dimensional modeling, positioned at 200 m downstream of the nozzle exit.

The translational temperature fields are compared in Fig. 4, obtained by two- and three-dimensional codes for the retrofiring configuration. There is a very good agreement between the two fields. A smaller computational domain was used for the three-dimensional case to lower the computational requirements because it was shown that the reduction does not affect the results. Because the two-dimensional solution was shown in our previous work to be particle and grid independent, the excellent agreement between two- and three-dimensional results proves that the computational requirements with respect to the number of particles and cells for the three-dimensional case are well satisfied.

## IV. Results and Discussion

### A. Application of the Overlay Technique to Steady Flows

Let us first consider the application of the proposed overlay technique to the calculation of OH($A$) radiation in a steady retrofiring flow. The principal coordinate-dependent parameters used in the overlay model are the velocities and density of the water species and the density of freestream atomic oxygen. The velocities of $H_2O$ in the $X$ and $Y$ directions are given in Fig. 5. Here, and in all subsequent results presented, the nozzle was located at $X = Y = 0$ m. The velocity in the $X$ direction (parallel to the plume direction)

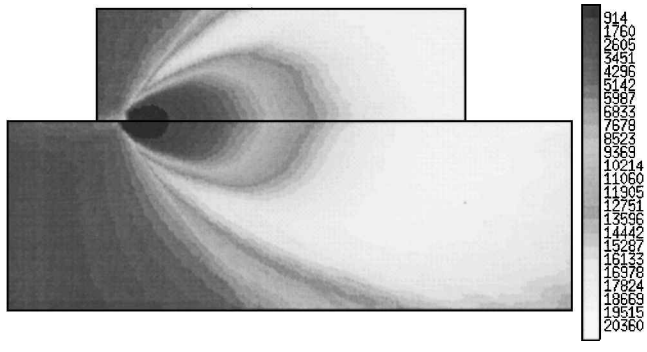


**Fig. 4 Total translational temperature (Kelvin) computed using three-dimensional (top) and axisymmetric (bottom) SMILE.**

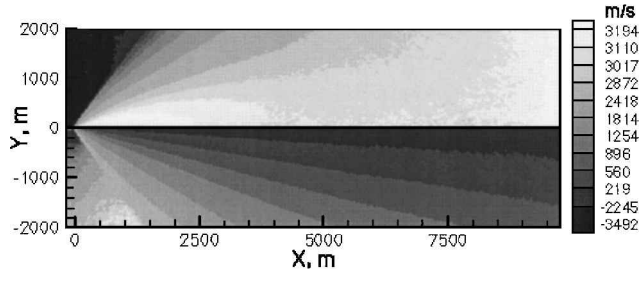


**Fig. 5 Parallel (top) and perpendicular (bottom) velocity profiles (meter per second) for water molecules (axes are given in meters in this and subsequent figures).**

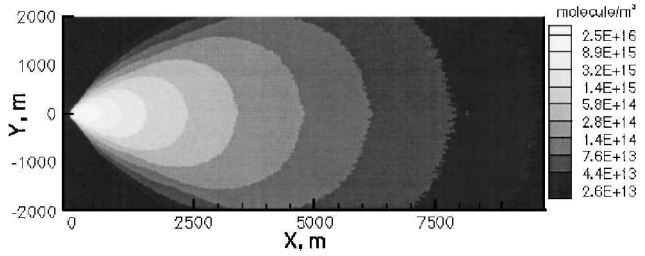


**Fig. 6 Contours of water number density in molecule per cubic meter.**

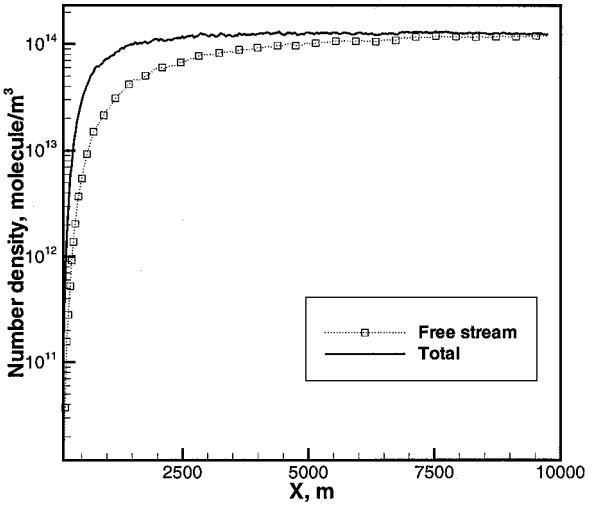


**Fig. 7 Number density profiles of total and freestream atomic oxygen along the plume axis.**

changes only within 1% in the region of the flow where the radiation is expected to be a maximum. The velocity in the $Y$ direction increases from 0 at the plume axis to 2 km/s at the periphery. Such an increase may cause only a small change in radiative emission. This is because the collision energy is proportional to the sum of the squares of relative velocity components, and a 2-km change in $Y$ component is, therefore, small compared to the maximum relative collision velocity in the $X$ direction of more than 10 km/s.

The water number density contours are shown in Fig. 6. Note a strong decrease in number density of $\sim 10^{22}$ molecule/m$^3$ at the nozzle exit to $4 \times 10^{16}$ molecule/m$^3$ at 500 m downstream. The $H_2O$ number density decreases about 200 times from 500 to 10 km downstream. The radiation is proportional to the product of the water and atomic oxygen densities. For oxygen, the ability to penetrate the plume is of great importance and will be discussed in detail later.

The mean atomic oxygen velocities in the overlay model are considered to be constant throughout the flow and to be equal to their freestream value. An important factor that influences the flow is the concentration of atomic oxygen. Because of a high plume density near the nozzle exit, O concentration drops dramatically in the vicinity of the nozzle. The total O number density profile along the plume axis is shown in Fig. 7. Again, $X = 0$ corresponds to the position of the nozzle.

Because the energy threshold of reaction (1) is high, the particles that are most likely to produce radiation are freestream oxygen atoms that have not collided with the plume. The oxygen atoms that previously collided with plume particles are less energetic and, therefore, give a smaller contribution to the reaction process. The number density of O not collided with plume (denoted as freestream) and the total O number density differ significantly, especially near the nozzle exit (Fig. 7). There was no freestream oxygen observed in calculations at distances less than 100 m from the nozzle due to high plume density in this region.

As a high-velocity component, the freestream oxygen is more important for the reaction under consideration; therefore, it is used in the overlay approach instead of the total atomic oxygen concentration. The application of the approach is shown in Fig. 8, where the number of radiative reactions is compared with that presented in our previous work and obtained by the traditional DSMC approach.[7] The statistical scatter is much lower for the overlay technique, whereas the computational time was about a factor of 10 shorter than for the full DSMC solution. An agreement between the two solutions is quite satisfactory, especially in the region where the radiation is a maximum.

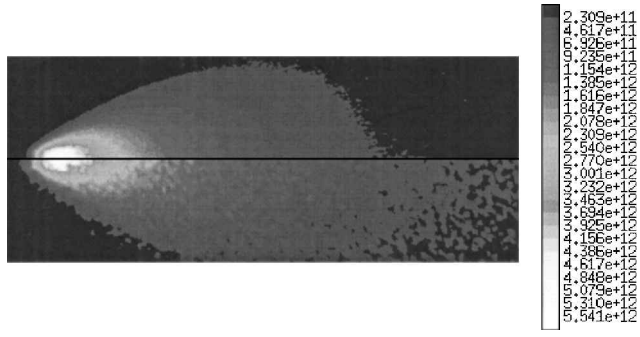

**Fig. 8 Number of radiative reactions per cubic meter per second for the overlay (top) and conventional DSMC (bottom) approaches; overlay and DSMC computational ranges were 2 × 10 and 5 × 15 km, respectively.**

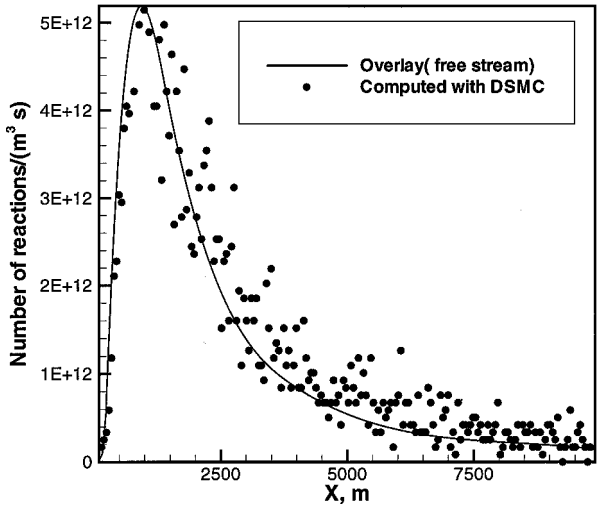


**Fig. 9 Comparison of overlay and DSMC radiance along the plume axis.**

A comparison of radiation profiles along the plume axis for the two approaches is given in Fig. 9 on a linear scale. Note that the unsmoothed DSMC data are shown here. The approximate (overlay) technique captures both the maximum location and magnitude quite accurately compared to the full DSMC results. In the far field (distances more than 3 km downstream), the values obtained by the overlay technique slightly underestimate those computed with the DSMC. Figure 9 shows that good agreement with the DSMC radiation solution along the plume axis is obtained if it is assumed that only freestream atomic oxygen that has not collided with the plume may react with water. If the total O number density is used, the radiation profiles are considerably higher (compare number densities in Fig. 7). Therefore, Fig. 9 shows that the freestream oxygen that has not collided with plume molecules gives the main contribution to OH($A$) radiation for a retrofiring geometry. Again, this is due to a large relative translational energy available in collisions between the freestream oxygen and plume molecules.

One of the advantages of the overlay technique is that it provides results with small statistical scatter in the periphery flow. The radiation profiles in a cross section parallel to the plume axis at $Y = 1900$ m are given in Fig. 10. The overlay data are smooth, whereas the DSMC solution has a very large statistical scatter due

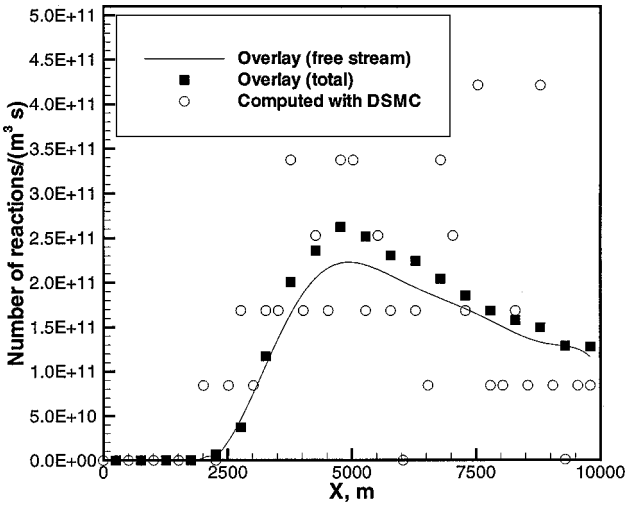


**Fig. 10 Radiation profiles at $Y = 1900$ m for different computational techniques.**

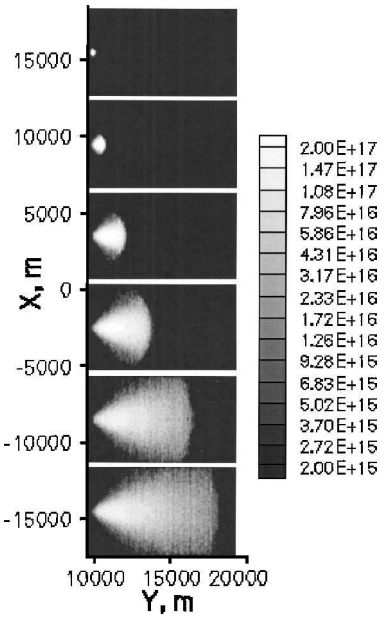


**Fig. 11 Transient behavior of radiation maps (number of radiative reactions per square meter per second) at a viewing angle of 90 deg with respect to the plume axis (time is 0.1, 0.3, 0.7, 1.2, 2.0, and 2.5 s from top to bottom). Each map covers a spatial domain of 10 × 4 km.**

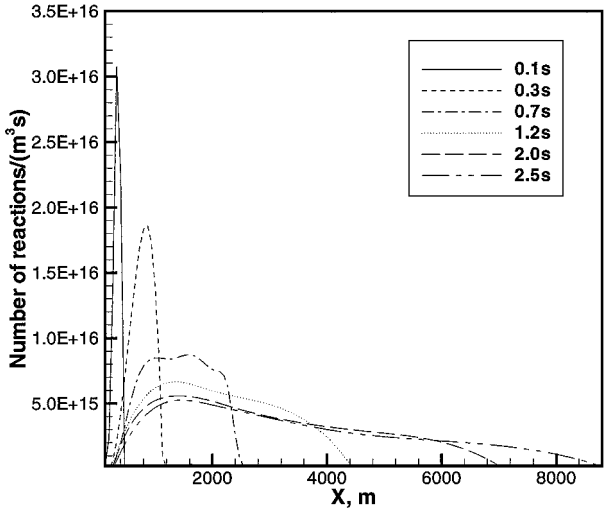


**Fig. 12 Temporal evolution of radiance profiles along the plume axis at viewing angle of 90 deg.**

to a low number of radiation events in the periphery. It would take much longer computational time for the full DSMC approach to obtain the small level of statistical scatter observed for the overlay technique. The difference between the overlay solutions using total and freestream oxygen number densities is much smaller than along the centerline because the plume number density is low in this region, and most of the oxygen atoms do not collide with the plume.

The main conclusion of this section is that the overlay technique enables one to model radiative emission credibly and, therefore, allows us to use it for examination of the unsteady, transient radiation phenomena.

### B. Modeling of the Flow Initiation Process

The overlay technique was used in this work to simulate the transient radiation structure observed during the first seconds of the PME retrofiring. In this set of computations, the axisymmetric SMILE code has been used with the total number of simulated molecules of about $3 \times 10^6$. This large a number of molecules was used to obtain reasonable statistics for computing the transient flow. The number of molecules in a typical macroparameter cell, in the region of maximum radiation, amounted to several hundreds. Macroparameters such as temperature and number density were sampled over 10 subsequent time steps for every desired transient time. The value of 10 time steps was chosen because the molecules, on average, do not cross more than one macroparameter cell during this time. During this time interval, their properties are still changing as a result of collisions. The total sample size for a given time moment is, therefore, several thousands, which turns out to be sufficient for our purpose of using macroparameters to calculate radiation.

The development of the glow pattern at different times is shown in Fig. 11. The results presented were obtained by integration along the line of sight with the viewing angle of 90 deg, that is, perpendicular to the direction of the plume. It is clearly seen that there is a sharp maximum in radiation observed in the vicinity of the nozzle at $t = 0.1$ s. Again, the radiation maximum is proportional to the product of the freestream oxygen and plume water number densities. The reason for the maximum at $t = 0.1$ s is that initially there is a large concentration of the freestream atomic oxygen in the region close to the nozzle that has not yet been evacuated by the relatively high-pressure plume. As the plume develops farther downstream (with the engine still firing), the dense core of the plume interferes with upstream oxygen penetration. The plume interference causes, in turn, a significant reduction of the maximum radiation, which will shift downstream to its steady-state location of about 1500 m from the nozzle exit. The radiation structure does not change significantly after the first 2 s of firing.

The quantitative illustration of the changing glow pattern after motor startup is shown in Fig. 12, where the profiles of the number of radiative reactions per cubic meter per second are plotted along the plume axis. Again, note a radiation maximum at $t = 0.1$ s that is more than six time larger than the radiation maximum at steady state. There is a decrease in the maximum after 0.3 s, with changes of only about 15% after the first second.

The time dependence of the radiation glow at a viewing angle of 172 deg is significantly different from the preceding case. The time history of radiation transient behavior for 172 deg is presented in Fig. 13. The principal difference is that the location of the radiation maximum hardly changes, and its value does not significantly decrease. This is because the number of reactions calculated by integration through the plume axis is weakly dependent on the penetration of the freestream oxygen upstream of the nozzle exit. The radiation emission spreads to the sides reaching the field of view boundary of 2 km in less than 2 s.

This transient radiation behavior was obtained using the Arrhenius rate parameters given in Table 2. The sensitivity of transient behavior to the chemical reaction rate was also examined. To

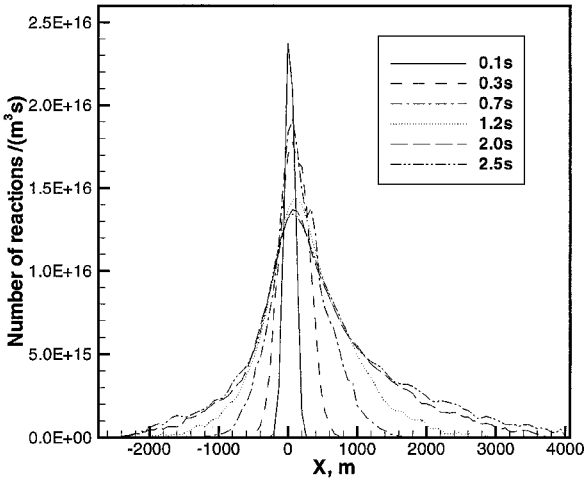


**Fig. 13 Temporal evolution of radiance profiles at a viewing angle of 172 deg.**

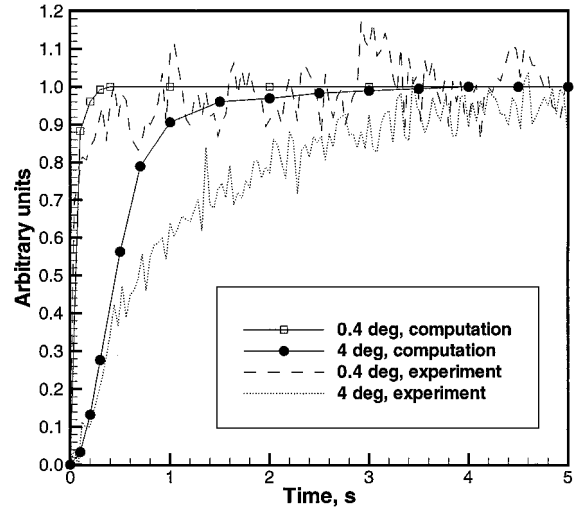


**Fig. 14 Comparison of transient simulation and experimental radiation profiles for different fields of view.**

this end, a computation first was performed for the reaction threshold reduced by a factor of two. Then, at the original reaction threshold, the value of $B$ was modified ($B = 1$ was used instead of 1.3). The main conclusion of those studies is that, although the absolute magnitude of radiative emission is different from the baseline case, the qualitative structure is very similar. Again, a sharp maximum is observed at $t = 0.1$ s, which decreases with time and space. The relative magnitude and position of the radiation maxima weakly depends on the reaction threshold.

An important reason for developing the overlay technique was to be able to compare simulations of the transient radiation emission with the data obtained from flight measurements. The viewing angle for these measurements was 172 deg. The experimental data for the transient flow were derived by the integration of radiation maps over various spatial regions (closer or farther away from the nozzle, which corresponds to different fields of view) at different times. The maximum radiance, in the vicinity of the nozzle, is attributed to other sources of radiation and was subtracted from the total emission.[12] The simulation results were obtained by integration over spatial regions corresponding to those used in analyzing the experimental data. Only a single radiation source is modeled in the simulations presented here [OH($A$)]. In contrast to the experimental data, there is no spatial restriction used in processing the computational results, and even regions close to the nozzle are included.

The comparison of calculated and measured radiance as a function of time is given in Fig. 14 for two different fields of view, 0.4 and 4 deg. The agreement between the experimental data and simulation

**Table 4 Elastic scattering models**

| Case designation | Description |
|---|---|
| $\alpha = 0.25$ | Baseline VHS model, $d$ from Ref. 3, $\alpha = 0.25$ |
| $\alpha = 0.0$ | Hard sphere model, same diameter as the baseline model |
| $\alpha = 0.5$ | Pseudo-Maxwellian molecular model |
| Increased diameters | Diameters increased by a factor of $\sqrt{10}$ relative to the baseline case, $\alpha = 0.25$ |

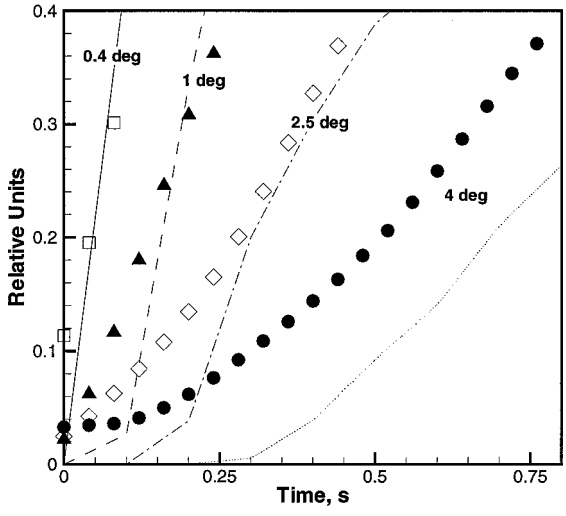


**Fig. 15 Temporal evolution of plume radiation at different lines of sight; lines denote computations, symbols experimental data.**

is quite satisfactory for the first 0.5 s after motor startup or computational initiation. At later times, the calculated values overpredict the experimental data. There could be several possible reasons for that, such as the accuracy of the data subtraction of brightest region as well as the existence of different or additional molecular sources of radiance than OH($A$).

Figure 15 presents the experimental and computed signal development along different lines of sight measured from the nozzle position. Four different fields of view are compared here, corresponding to the angles of 0.4, 1, 2, and 4 deg. The results show a slightly higher slope predicted in the computations for the smaller angles, again possibly due to the reasons discussed earlier. The qualitative agreement is quite good considering that the simulation does not utilize any motor transient behavior that may also account for these differences.

### C. Sensitivity of Radiation to the Total Collision Cross Section

In our previous work[2] we showed that the radiation magnitude predicted by the the total collision energy (TCE)[3] model was sensitive to the number of internal degrees of freedom assumed. The location of the radiation maximum and the radiation spatial distribution was found to be insensitive to changes in the TCE model. In this work we investigate the sensitivity of the radiation spatial distribution to the elastic scattering total cross section using the overlay technique. The authors of Ref. 13 have shown that there is an important uncertainty in the elastic scattering cross section parameters for high-energy collisions. In the VHS model used here, there are two principal parameters that determine the interaction: the molecular diameter $d$ and the exponent in the viscosity–temperature dependence $\alpha$ ($\mu \propto T^{0.5+\alpha}$). In addition to the baseline model that uses diameter values from Ref. 3 and one value of $\alpha = 0.25$ for all species, simulations were performed for three additional cases, summarized in Table 4. The baseline model appears to be the most reliable, but still there is a significant uncertainty in the magnitude of the molecular diameter and the exponent in the viscosity–temperature dependence for high-velocity collisions modeled in this work. Large variations of these parameters were, therefore, taken to understand their possible impact on the predicted radiation.

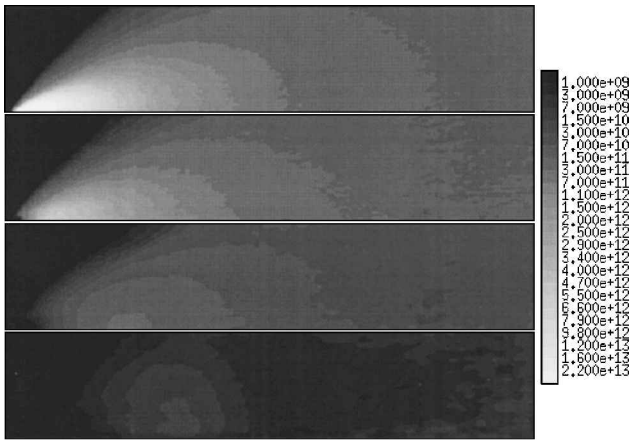


**Fig. 16 Radiation maps in number of reactions per cubic meter per second for different parameters of the VHS model; from top to bottom: $\alpha = 0.5$, $\alpha = 0.25$, and $\alpha = 0.0$; increased diameters. Each map covers a spatial domain of 10 × 2 km.**

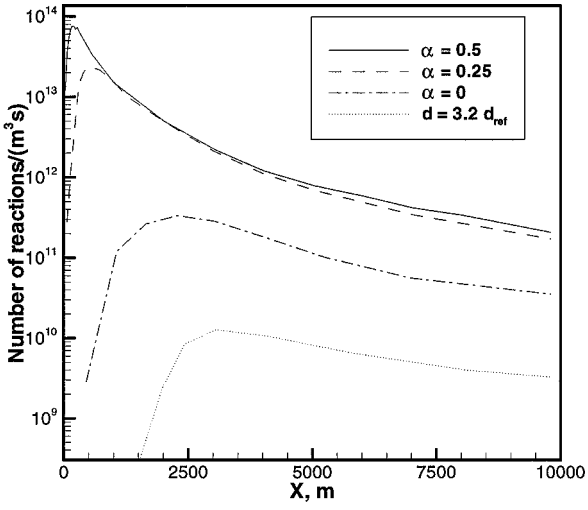


**Fig. 17 Number of radiation reactions profiles along the plume axis for different VHS parameters.**

The ability of freestream atomic O to penetrate upstream through the plume toward the nozzle exit increases for decreasing total collisional cross section or increasing $\alpha$. The computations show that, although many of the freestream oxygen atoms reach the nozzle exit for the pseudo-Maxwellian case, none come closer than 300 m for the hard sphere model. Accordingly, the penetration is less for the case of increased particle diameters.

As was seen earlier, the penetration issue plays a determining role in the radiation process. The radiation fields are presented in Fig. 16 for the four total collisional cross section models given in Table 4. The maximum radiation is observed for pseudo-Maxwellian molecules (top plot in Fig. 16). In this case, the maximum is located less then 200 m from the nozzle, where both the water and oxygen densities are high enough. For the $\alpha = 0.25$ model, the radiation maximum decreases and shifts downstream relative to the pseudo-Maxwellian model. For the other two cases, the gradients of the radiation field are smoother, and the radiative emission is significantly lower. As expected, the case of increased diameters (with a higher total cross section) results in the lowest radiative emission.

To compare quantitatively the radiance spatial distribution for the four cases, radiation profiles taken along the plume axis and the plume periphery are presented in Figs. 17 and 18, respectively. The plume periphery distribution is shown along the line parallel to the plume axis and positioned at $Y = 1500$ m. The number of radiative reactions is a maximum for $\alpha = 0.5$, with a value of

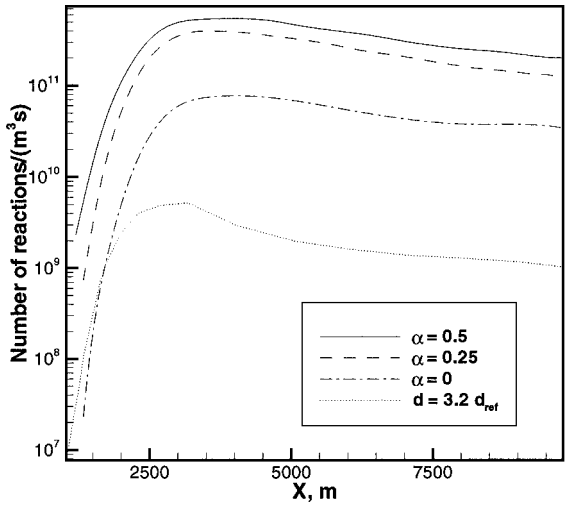


**Fig. 18 Number of radiation reactions profiles at $Y = 1500$ m for different VHS parameters.**

$8 \times 10^{13}$ molecule/(m$^3$s) at 200 m downstream from the nozzle. The maximum for $\alpha = 0.25$ is about three times lower and is located about 1 km. For these two cases, the radiation values are similar for distances larger than 1 km. The radiance for $\alpha = 0.0$ is several orders of magnitude lower than for the first two cases at $X < 2000$ m and about 10 times lower for $X > 3000$ km. The lowest values were obtained for the increased diameter case. Similar trends among the different elastic scattering models are observed for the plume periphery (Fig. 18).

The results presented in this section illustrate the importance of using an adequate model for intermolecular interactions because it substantially affects the radiation fields both in term of magnitude and location of the maximum. The choice of a relevant model is complicated for very high-energy collisions, where there is a lack of both experimental and analytical data. The range in the results of Figs. 17 and 18 also show that the overprediction of the simulations in earlier work[2] compared to the data may be reduced by a different choice of elastic scattering model.

### D. Modeling of Three-Dimensional Flows

The results presented in the preceding sections are related to the retrofiring configuration. In that case, the flow has a symmetry axis coincident with the plume axis and can be simulated using an axisymmetric, that is, essentially two-dimensional, model. For an angle of attack different from 180 deg, a three-dimensional model has to be used. In this work, the calculations were performed with the number of molecules and collision cells of 2 and $10 \times 10^6$ respectively. Full DSMC simulations were performed instead of using the overlay technique in this case. The application of the overlay technique is more complicated for small angles of attack than for the retrofiring configuration. Whereas only freestream molecules need to be included for the retrofiring configuration, for smaller angles of attack the O atoms that have already collided with the plume contribute to the radiation process. Therefore, a correction would be necessary to the overlay analysis presented earlier to include those collided molecules that have temperature and velocities different from those of the freestream. The implementation of such a correction, however, is not straightforward and, therefore, was not pursued.

Consider first the impact of the angle of attack variation on the OH radiation. Figure 19 shows maps of the number of reactions per square meter per second, which is directly proportional to the OH($A$) radiance, for different angles of attack. These values were obtained by the integration of the number of reactions per unit volume per unit time through the direction perpendicular to the $XY$ plane. It can be seen that the counterflow geometry (top) generates the largest region of radiation. Approximately 30–40% of the collisions in the counterflow geometry meet the threshold energy criteria. As the

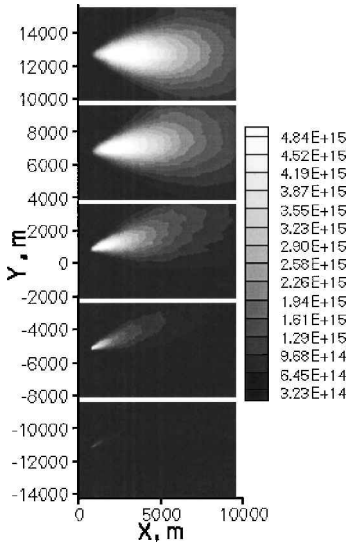


**Fig. 19 Comparison of number of reactions of reaction (1) to form OH($A$) per square meter per second for angles of attack of 100 (bottom), 120, 140, 160, and 180 deg (top).**

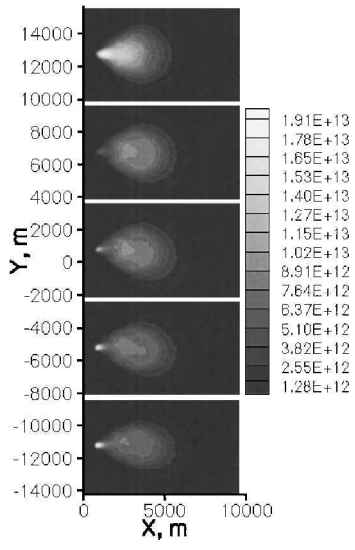


**Fig. 21 Comparison of number of reactions of reaction (2) to form NH($A$) per square meter per second for angles of attack of 100 (bottom), 120, 140, 160, and 180 deg (top).**

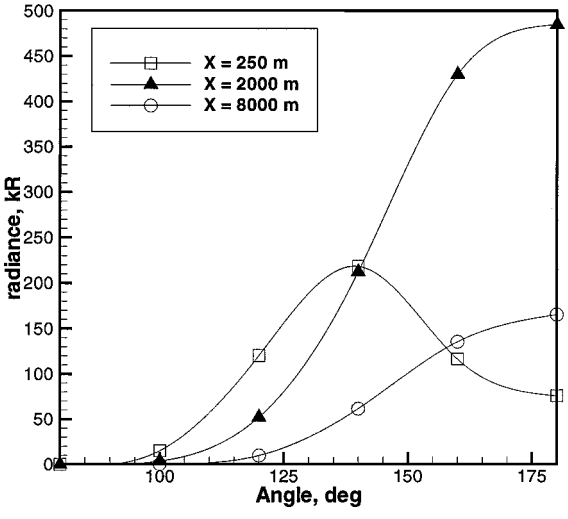


**Fig. 20 OH($A$) radiation in the flow at different angles of attack for three locations along the plume axis.**

angle of attack is reduced, the radiation decreases. This is because the energy threshold for reaction (1) is high, and in the counterflow case it is more likely for the colliding particles to have a relative energy that exceeds the threshold. The number of countercollisions decreases with decreasing angle of attack, and the location of the radiation cloud shifts toward the freestream direction.

Figure 20 provides a more detailed analysis of the values of radiance calculated at three different locations downstream of the nozzle exit: in the near field ($X = 250$ m), at the location where the radiation has a maximum at 180 deg ($X = 2000$ m), and in the far field ($X = 8000$ m), with the nozzle being positioned at $X = 0$. Consistent with Fig. 19, the absolute maximum of radiation was observed at $X = 2000$ m for the retrofiring configuration. The radiance gradually decreases with decreasing angle of attack for $X = 2000$ and 8000 m, whereas there is a maximum at about 140 deg for the near-field location. The maximum is related to the combined effect of two factors. The first is the penetration of the freestream atomic oxygen upstream toward the nozzle, where the water number density is a maximum. Penetration toward the nozzle is better for smaller angles, therefore increasing the radiation. Note that the first factor is important only for the portion of the flow close to the nozzle, where the density is high. The second factor is the relative collision velocity that depends on the direction of water and oxygen velocities. The relative collision velocity decreases for smaller angles resulting in a decrease in radiation.

Earlier results considered the UV radiation as a result of reaction (1). The second possible radiator in the UV range is NH($A$) formed by reaction (2). The radiation due to this mechanism was studied for the retrofiring configuration in Ref. 2, where it was found that the spatial distribution of the radiation was spherical and closer to the nozzle exit plane than that of OH($A$). Here, we consider the change of the NH($A$) radiation map for different angles of attack. The Arrhenius constants used for reaction (2) are given in Table 2. Figure 21 shows that for all angles the radiation maximum is located closer to the nozzle exit than was predicted for OH($A$). Unlike water dissociation, there is ample relative collisional energy to form NH($A$). A smaller reaction threshold causes a difference in the shape of NH($A$) radiation clouds as compared to OH($A$). Again, the location of the radiation maximum is dependent on the penetration depth of atomic O into the plume. For the counterflow geometry, the majority of the radiation is located approximately 700 m downstream of the nozzle. The total number of reactions is proportional to the product of the O atom and hydrazine fragment number densities and the reaction cross section. As the angle of attack is decreased, the regions of bright radiation also decrease, relative to 180 deg. This is due to the decrease in the reaction cross section as the relative collisional energy is reduced. However, for smaller angles of attack the plume shielding is reduced, and the atomic O can penetrate closer to the nozzle. The progression of contour plots from 180 to 100 deg angle of attack in Fig. 21 shows how the radiation field changes with these two competing affects. At the 120-deg angle of attack, the bright region is now shifted to the left to 250 m from the nozzle. The important conclusion is that the NH($A$) radiation does not decrease as strongly with angle of attack as that from OH($A$), due to a large difference in the activation energies for the two reaction paths.

The quantitative dependence of NH($A$) radiance on the angle of attack is shown in Fig. 22 for three different locations downstream of the nozzle exit [similar to that for OH($A$)]. The difference between the dependence for NH($A$) and OH($A$) is attributed to the appearance of the NH($A$) total radiation maximum in the vicinity of the nozzle exit at the angles of attack of about 90 deg. This maximum is due to the low-energy threshold of reaction (2). Note that our results qualitatively agree with the experimental data[1] obtained for three different locations of 4, 10, and 33 m. Because of inadequate grid resolution close to the nozzle, we are not able to choose values closer to the nozzle exit. However, the closest of our calculations (at 250 m from the nozzle) has a very similar functional form as the measurements given in Ref. 1. They also agree well on an absolute

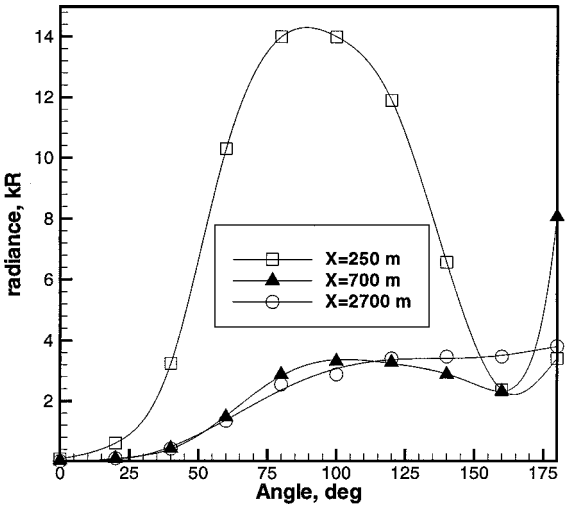


**Fig. 22 NH($A$) radiation in the flow at different angles of attack for three locations along the plume axis.**

scale with a maximum of 14 k$Ra$ at 250 m for in the DSMC simulation and ~27 k$Ra$ at 33 m for the data, where $Ra$ is a unit of radiation, Rayleigh $= 10^6$ photon/cm$^2$s.

## V. Conclusions

The numerical study of radiation phenomena due to the interaction of a hydrazine plume with the ambient atmosphere at 380 km was conducted using the DSMC method. Two numerical techniques for modeling radiation from chemically reacting rarefied plume flows were presented and applied to the MirEx and shuttle GLO conditions. The work was aimed at modeling the radiative emission from OH($A$), produced as a result of high-energy interactions of water molecules from the plume with the freestream atomic oxygen, in transient, steady-state, and three-dimensional flows. The angular variation of the OH($A$) radiation was contrasted with that of NH($A$), another important UV radiator present in hydrazine space plumes. The computational analysis and comparisons with experimental data established a consistent set of parameters for the DSMC numerical approach that can be used to model a complex problem.

Because the direct use of the DSMC approach to model the time-dependent initiation of the plume radiation is computationally prohibitive, an overlay technique was implemented to analyze the transient evolution of the OH($A$) glow. This technique makes use of macroparameters obtained by the DSMC method, and the results are validated for a steady-state flow by a comparison with the DSMC solution.

The transient pattern of OH($A$) radiation was examined for the retrofiring configurations at different viewing angles. The importance of accurate modeling of the freestream oxygen penetration upstream toward the nozzle was shown. A comparison of the measured time evolution with modeling during the first seconds after firing was performed. Although the radiation spatial profiles are similar for the first 0.5 s, a significant difference was observed from 1 s on. The influence of the reaction rate was also examined and found to affect weakly the transient spatial distribution of the glow, for the range of parameters considered. It is possible that modeling of other transients related to motor performance are required to resolve the remaining discrepancies between modeling and data.

The impact of the molecular total collision model on the steady-state radiance was examined using the overlay technique. A large difference both in radiation magnitude and shape was found for different molecular diameters and temperature exponents of the coefficient of viscosity. Additional analysis is needed to better define the elastic scattering cross sections for high-energy collisions.

The starting surface–three-dimensional modeling provided insight into the atomic oxygen penetration as a function of angle of attack and qualitative comparison with the shuttle GLO data. The radiation field produced by NH($A$) is almost symmetric with the respect to the plume axis for angles of attack of 100 deg and higher. The maximum radiation shifts from 700 m at 180 deg to about 200 m for angles of attack of 140 deg and smaller. Moreover, the global maximum of NH($A$) emission is observed for the angle of about 100 deg, and it is almost two times larger than that for 180 deg. The computational results agree qualitatively with the shuttle GLO measurements. The variation in the OH($A$) radiation spatial distribution as a function of angle of attack is much greater than for NH($A$). This sensitivity may be attributed to the higher activation energy.

## Acknowledgments

The work at George Washington University and the Pennsylvania State University was supported by the Army Research Office Grant DAAG55-98-1-009, the Air Force Office of Scientific Research (AFOSR) Grant F49620-99-1-0143, and the Ballistic Missile Defense Organization. The work at TsNIIMASH was supported by the Russian Aerospace Agency and AFOSR.

## References

[1] Viereck, R. A., Murad, E., Knecht, D. J., Pike, C. P., Bernstein, L. S., Elgin, J. B., and Broadfoot, A. L., "The Interaction of the Atmosphere with the Space Shuttle Thruster Plume: The NH(A-X) 336-nm Emission," *Journal of Geophysical Research*, Vol. 101, No. A3, 1996, pp. 5371–5380.

[2] Gimelshein, S. F., Levin, D. A., Drakes, J. A., Karabadzhak, G. F., and Ivanov, M. S., "Ultraviolet Radiation Modeling from High Altitude Plumes and Comparison with Mir Data," *AIAA Journal*, Vol. 38, No. 9, 2000, pp. 2344–2352.

[3] Bird, G. A., *Molecular Gas Dynamics and the Direct Simulation of Gas Flows*, Clarendon, Oxford, England, U.K., 1994, pp. 208–217.

[4] Baulch, D. L., Drysdale, D. D., Home, D. G., and Lloyd, A. C., *Evaluated Kinetic Data for High Temperature Reactions, 1, Homogeneous Gas Phase Reactions of the $H_2$–$O_2$ System*, Butterworths, 1972, pp. 109–118.

[5] Drakes, J. A., Swann, D. G., Karabadzhak, G. F., and Plastinin, Y., "DSMC Computations of the Progress-M Spacecraft Retrofiring Exhaust Plume," AIAA Paper 99-0975, Jan. 1999.

[6] Ivanov, M. S., Markelov, G. N., and Gimelshein, S. F., "Statistical Simulation of Reactive Rarefied Flows: Numerical Approach and Applications," AIAA Paper 98-2669, June 1998.

[7] Levin, D. A., Gimelshein, S. F., Drakes, J. A., Hiers, R. S., Karabadzhak, G. F., and Plastinin, Y., "Modeling of the Emissions from the Soyuz, Progress, and Mir Rocket Exhaust Plumes at High Altitudes," AIAA Paper 2000-0601, Jan. 2000.

[8] Bird, G. A., "Monte-Carlo Simulation in an Engineering Context," *Rarefied Gas Dynamics*, edited by S. Fisher, Vol. 74, Progress in Astronautics and Aeronautics, AIAA, New York, 1981, pp. 239–255.

[9] Borgnakke, C., and Larsen, P. S., "Statistical Collision Model for Monte Carlo Simulation of Polyatomic Gas Mixture," *Journal of Computational Physics*, Vol. 18, No. 4, 1975, pp. 405–420.

[10] Parker, J. G., "Rotational and Vibrational Relaxation in Diatomic Gases," *Physics of Fluids*, Vol. 2, No. 4, 1959, pp. 449–462.

[11] Millikan, R. C., and White, D. R., "Systematics of Vibrational Relaxation," *Journal of Chemical Physics*, Vol. 39, No. 12, 1966, pp. 3209–3213.

[12] Karabadzhak, G., Plastinin, Y., Drakes, J., McGregor, W., Bradley, D., Teslenko, V., Shvets, N., Volkov, O., Kukushkin, V., Gimelshein, S., and Levin, D., "Mir-Based Measurements of the Ultraviolet Emissions from Rocket Exhaust Plume Interactions with the Atmosphere at 380-km Altitude," AIAA Paper 2000-0105, Jan. 2000.

[13] Erofeev, A. I., Friedlander, O. G., Karabadzhak, G. F., and Plastinin, Y. A., "Comparison of Monte-Carlo Modeling and Experimental Results of UV-Emission from Engine Exhaust Plume Interacting with Upper Atmosphere," *Proceedings of the 22nd International Symposium on Rarefied Gas Dynamics*, 2000 (to be published).